Available online at www.sciencedirect.com
SCIENCE DIRECT
ELSEVIER
Thin Solid Films 496 (2006) 247 – 252
thin solid films
www.elsevier.com/locate/tsf

# ArF-line high transmittance attenuated phase shift mask blanks using amorphous $Al_2O_3$–$ZrO_2$–$SiO_2$ composite thin films for the 65-, 45- and 32-nm technology nodes

Fu-Der Lai [a,*], Jui-Ming Hua [a,b], C.Y. Huang [c], Fu-Hsiang Ko [d], L.A. Wang [e], C.H. Lin [c], C.M. Chang [c], S. Lee [c], Gia-Wei Chern [e]

[a] *Institute of Electro-Optical Engineering, National Kaohsiung First University of Science and Technology, Kaohsiung 811, Taiwan*
[b] *Automation Department, Metal Industries Research and Development Centre, Kaohsiung 811, Taiwan*
[c] *Department of Materials Engineering, Tatung University, Taipei 104, Taiwan*
[d] *National Nano Device Laboratories, 1001-1, Ta-Hsueh Rd, Hsinchu 300, Taiwan*
[e] *Department of Electrical Engineering and Institute of Electro-Optical Engineering, National Taiwan University, Taipei 107, Taiwan*

Received 7 March 2005; received in revised form 9 August 2005; accepted 22 August 2005
Available online 9 November 2005

**Abstract**

Amorphous $(ZrO_2)_x$–$(SiO_2)_{1-x}$ and $(Al_2O_3)_x$–$(ZrO_2)_y$–$(SiO_2)_{1-x-y}$ composite films were prepared using r.f. unbalanced magnetron sputtering in an atmosphere of argon and oxygen at room temperature. The $(ZrO_2)_x$–$(SiO_2)_{1-x}$ and $(Al_2O_3)_x$–$(ZrO_2)_y$–$(SiO_2)_{1-x-y}$ composite films were completely oxidized when an $O_2$/Ar flow rate ratio of 2.0 was used. The optical constants of these thin films depend linearly on the mole fraction of corresponding films. By tuning the $(x, y)$ mole fractions of ($Al_2O_3$, $ZrO_2$) in the $(Al_2O_3)_x$–$(ZrO_2)_y$–$(SiO_2)_{1-x-y}$ composite films, the optical constants can meet the optical requirements for a high transmittance attenuated phase shift mask (HT-AttPSM) blank. The $n-k$ values in the quadrangular area in the $(x, y)$ plane, where $x$ and $y$ represent the mole fractions of $Al_2O_3$ and $ZrO_2$, respectively, meet the optical requirements for an HT-AttPSM blank with an optimized transmittance of $20 \pm 5\%$ in ArF lithography. It is noted that the quadrangular area is bounded by (0, 0.31), (0, 0.62), (0.26, 0) and (0.57, 0). All the films also met the chemical and adhesion requirements for an HT-AttPSM application. One $(Al_2O_3)_{0.1}$–$(ZrO_2)_{0.52}$–$(SiO_2)_{0.38}$ composite film was fabricated with optical properties that meet the optimized optical requirements of ArF-line HT-AttPSM blanks. Combined with these HT-AttPSMs, ArF-line (immersion) lithography may have the potential of reaching 65-, 45-nm and possibly the 32-nm technology nodes for the next three generations.
© 2005 Elsevier B.V. All rights reserved.

*Keywords:* High transmittance attenuated phase shift mask; ArF-exposure-line lithography; Amorphous composite film; Optical properties

## 1. Introduction

The destructive interference of light at the edges of circuit features during photolithography is always a critical issue [1]. The usage of attenuated phase shift mask (AttPSM) technology has the potential capability to improve both the depth of focus and the resolution [2]. Without the phase conflict problem for arbitrary mask [3], it is easier to fabricate AttPSM than other types of phase shift masks. As a result, AttPSM is one of the most important techniques for extending the ArF-exposure-line photolithography to a new generation with a less than 100-nm resolution. It is known that high-transmittance-AttPSMs (HT-AttPSMs) have better depth-of-focus and resolution than general AttPSMs. However, due to the strong side-lobe effect of HT-AttPSMs, they have not been used in the lithography processes. With improved photoresist technology and added Cr-assisted features [4], the side-lobe effect can be minimized and the focus margin can be increased. Thus, combined with a HT-AttPSM, ArF-line lithography may have the potential of reaching a 65-nm technology node [5] and ArF-line immersion lithography may have the potential of reaching the 45-nm and possibly the 32-nm technology nodes for the next three generations.

A typical HT-AttPSM thin film features a transmittance of $20 \pm 5\%$, a reflectance of less than 20%, and a $\pi$-phase shift at the exposure wavelength. There have been many material

* Corresponding author.
*E-mail address:* fdlai@ccms.nkfust.edu.tw (F.-D. Lai).

0040-6090/$ - see front matter © 2005 Elsevier B.V. All rights reserved.
doi:10.1016/j.tsf.2005.08.382

candidates, such as MoSiO [6], $SiN_x$ [7], CrAlO [8], ZrSiO [9], CrN/AlN [10] and $Al_2O_3/Cr_2O_3$ [11] reported for AttPSM at a wavelength of 193 nm. These materials may also be used as HT-AttPSM blank materials. Some materials have a superlattice structure [10,11] which provides a wide tuning capacity range for the optical constants. However, the layer thickness in the AttPSM superlattices must be accurately controlled and the corresponding deposition processes are complicated. On the other hand, amorphous composite films having the tunable optical constants [12] are widely used in the preparation of optical devices such as antireflection coatings and notch filters. Moreover, a composite film is more easily fabricated than a superlattice thin film. We have previously used $ZrO_2-Al_2O_3$ composite thin films as HT-AttPSM blank layers [13]. It is expected that the optical constants of these three-component composite films would be tunable over a wide domain. Here we consider $ZrO_2-SiO_2-Al_2O_3$ composite films as HT-AttPSM blank layers. It has been demonstrated that $SiO_2$, $ZrO_2$ [14] and $Al_2O_3$ [15] thin films exhibit very good chemical inertness and optical characteristics. They have been widely used as optical coating layers. However, they have not yet been reported on the HT-AttPSM blank layers being used in ArF lithography.

In this study, $(Al_2O_3)_x-(ZrO_2)_y-(SiO_2)_{1-x-y}$ composite films were fabricated to meet the optical requirements of an HT-AttPSM blank layer, for working in ArF lithography. Amorphous $Al_2O_3$, $ZrO_2$ and $SiO_2$ thin films and $(Al_2O_3)_x-(ZrO_2)_x-(SiO_2)_{1-2x}$ composite films were prepared and their optical constants were studied. The dependence of the optical constant on the $ZrO_2$ mole fraction $x$ was also studied and was shown to meet the effective medium approximation (EMA). Furthermore, the optical constants of the $(Al_2O_3)_x-(ZrO_2)_x-(SiO_2)_{1-2x}$ composite films, consisting of three components, $Al_2O_3$, $ZrO_2$ and $SiO_2$, were also measured and again shown to conform to the EMA. One ($Al_2O_3$, $ZrO_2$) mole fraction domain was obtained for $(Al_2O_3)_x-(ZrO_2)_y-(SiO_2)_{1-x-y}$ composite films which meets the optical requirements of a HT-AttPSM blank. A $(Al_2O_3)_x-(ZrO_2)_y-(SiO_2)_{1-x-y}$ composite film sample was fabricated to meet the optical requirements of an HT-AttPSM blank with a transmittance of 18–20% and π-phase shift. The surface roughness and adhesion analysis were also studied.

## 2. Experimental details

### 2.1. Deposition process

$(ZrO_2)_x-(SiO_2)_{1-x}$ and $(ZrO_2)_x-(Al_2O_3)_y-(SiO_2)_{1-x-y}$ composite films were deposited on UV grade fused silica substrates ($n=1.561$ at 193 nm) and Si wafers by using r.f. reactive unbalanced magnetron sputtering in an atmosphere of Ar and $O_2$ at room temperature. Since a higher ion density can be obtained for an unbalanced magnetron sputtering system than a balanced one [16], a denser thin film can be obtained. Targets were made from pressed $ZrO_2$ (99.995% pure), $SiO_2$ (99.999% pure) and $Al_2O_3$ (99.999% pure) powders. The mixed powders were sintered at 800 °C for 4 h, then slowly cooled to room temperature. The $SiO_2$ mole fractions of the $(ZrO_2)_x-(SiO_2)_{1-x}$ target were 0%, 20%, 40%, 60%, 80% and 100%. The $SiO_2$ mole fractions of the $(Al_2O_3)_x-(ZrO_2)_x-(SiO_2)_{1-2x}$ target were 0%, 10%, 20%, 30%, 40%, 50%, 70% and 100%, respectively. In addition, the $Al_2O_3$ mole fractions of the $(Al_2O_3)_{1-2x}-(ZrO_2)_x-(SiO_2)_x$ target were 0%, 20%, 40%, 60%, 80% and 100%, respectively. The UV grade fused silica substrates had a surface flatness of $\lambda/10$ ($\lambda=632.8$ nm). The substrates were rotated during the deposition process to yield uniform thin films. The substrates were cleaned in an ultrasonic bath by a series of processes: in trichlorethane for 50 min; in deionized (D.I.) water for 10 min; in acetone for 5 min; in D.I. water for 10 min; in ethanol for 5 min; and in D.I. water for 10 min. The deposition chamber was surrounded by heating girdles. It was evacuated to a base pressure of less than $1\times10^{-6}$ Torr using a cool trap and a diffusion pump. Prior to deposition, the target was pre-sputtered for 20 min at 1.62 Pa Ar pressure to remove any $SiO_x$ ($x<2$), $ZrO_y$ ($y<2$) and $AlO_z$ ($z<1.5$) contaminants from the target erosion track, then for 1 h under the deposition parameters of the film, to fix the properties of the film. The gas flow rate was accurately measured to better than 0.1 sccm and was controlled by mass flow meter. All films were deposited according to the following parameters: 1.08 Pa pressure; 10 sccm Ar flow rate; 20 sccm $O_2$ flow rate; and 80 W sputtering power. The deposition rates were ~ 0.013 nm/s. Thickness was controlled to ~ 85 nm by using a quartz crystal microbalance monitor. All the deposited thin films were amorphous structure after characterization with high power X-ray diffraction (XRD) (MAC Science, M21X X-ray diffractometer) utilizing Cu Kα radiation of wavelength 0.154 nm. The step time and the step angle were 1 s and 0.02°. The chemical bonding states and composition of the thin films were examined by the X-ray photoelectron spectroscopy (XPS) (Perkin-Elmer Corporation, Minnesota, USA) and a Mg Kα X-ray (1253.6 eV) source operated at 15 kV and 20 mA. The vacuum of the chamber was less than $10^{-8}$ Torr. Before the XPS examination, each film was pre-sputtered by utilizing 2 keV $Ar^+$ ion sputtering for 1 min to eliminate any possible contaminations on the film surface.

### 2.2. Optical constant measurement

Because the extinction coefficient $k$ of the films is less than $10^{-4}$ at a wavelength of 632.8 nm, the film thickness and refractive index $n$ can be measured using an ellipsometer with a He–Ne laser. The transmittance and reflectance spectra in the 190–700-nm wavelength range were measured by an optical spectrometer (Hitachi, U3501) and averaged over 10 measurements. The refractive index $n$ and extinction coefficient $k$ of the films were obtained at various wavelengths, by the reflection-transmittance (R-T) method, in which multiple reflection effects were taken into account using the obtained R-T data [17].

### 2.3. Surface roughness and adhesion analysis

The chemical durability of the $(ZrO_2)_x-(SiO_2)_{1-x}$ and the $(Al_2O_3)_x-(ZrO_2)_y-(SiO_2)_{1-x-y}$ composite films was measured after being placed in the 90 °C solution (90% 10 M

$H_2SO_4$ + 10% $H_2O_2$) for 1 h and then in another 50 °C solution (1 M KOH) for 30 s. The surface roughness of the films before and after the chemical durability testing was measured using atomic force microscopy (AFM) (Digital Instruments, D3100) in the tapping mode with an etched silicon cantilever having a tip radius of 10 nm and apex angle of 35°. The AFM was set on the optical table (IDE, ETC-10LM2), which acted as an active isolation system. Scan speed is 0.4 μm/min. Sampling rate is 1 Hz. The adhesion between the composite films and the UV grade fused silica was analyzed using the ASTM Crosshatch tape testing method [18].

## 3. Results and discussion

### 3.1. Structure and chemical composition of composite films

As deposited, all thin films measured by XRD are amorphous. Variations in the transmittance are small when the $O_2$/Ar flow rate ratio exceeds 1, since the composite thin films will be nearly completely oxidized. This result is much like the result of our previous report [13].

In the $(Al_2O_3)_x$–$(ZrO_2)_y$–$(SiO_2)_{1-x-y}$ composite films, binding energies of Zr $3d_{5/2}$, Si 2p and Al $2p_{3/2}$ are identified by XPS in accordance with the XPS spectra [19] of $ZrO_2$, $SiO_2$ and $Al_2O_3$ when the $O_2$/Ar flow rate ratio is equal to 2. The ratios of O/Zr, O/Si and O/Al in $ZrO_2$, $SiO_2$ and $Al_2O_3$ thin films identified by XPS are 1.98 ± 0.11, 1.98 ± 0.05 and 1.51 ± 0.07, respectively. Thus, the deposited $(ZrO_2)_x$–$(SiO_2)_{1-x}$ and $(Al_2O_3)_x$–$(ZrO_2)_y$–$(SiO_2)_{1-x-y}$ composite films are stoichiometric. The film composition ratios of Al/Zr/Si are dependent on the area ratios of XPS spectra at binding energies of Al $2p_{3/2}$, Zr $3d_{5/2}$ and Si 2p. The film composition ratios of Al/Zr/Si are obtained. The film composition is nearly equal to the target composition. In the following discussions, the $O_2$/Ar flow rate ratio is set to be 2.

### 3.2. Optical constants of $(ZrO_2)_x$–$(SiO_2)_{1-x}$ and $(ZrO_2)_x$–$(Al_2O_3)_{1-x}$ composite films

The transmittance and reflectance spectra of $(ZrO_2)_x$–$(SiO_2)_{1-x}$ composite films are shown in Fig. 1(a). The decrease in transmittance for $\lambda < 200$ nm with an increasing $ZrO_2$ mole fraction is due to the higher absorption of $ZrO_2$ compared with that of $SiO_2$. Regarding the reflection spectra, there is a peak reflectance when the wavelength is less than 300 nm for each sample. The higher the $ZrO_2$ mole fraction, the higher the value of the reflectance peak is. The corresponding peak wavelength decreases as the $ZrO_2$ mole fraction increases. The overall reflectance increases more or less with the increasing $ZrO_2$ ratio. The dependence of the refractive index and the extinction coefficient of $(ZrO_2)_x$–$(SiO_2)_{1-x}$ composite films, with different $ZrO_2$ mole fraction on the wavelength is shown in Fig. 1(b) and (c), respectively. As can be seen, a higher $ZrO_2$ mole fraction results in a higher refractive index and a higher extinction coefficient when $\lambda < 250$ nm. However, the extinction coefficient is less than $10^{-4}$ when $\lambda > 300$ nm. Fig. 2 illustrates the variation in the optical constants at $\lambda = 193$ nm, as a function of the $ZrO_2$ mole fraction, for the $(ZrO_2)_x$–$(SiO_2)_{1-x}$ composite films shown in Fig. 1(b). The refractive indices increase when the $ZrO_2$ mole fraction increases.

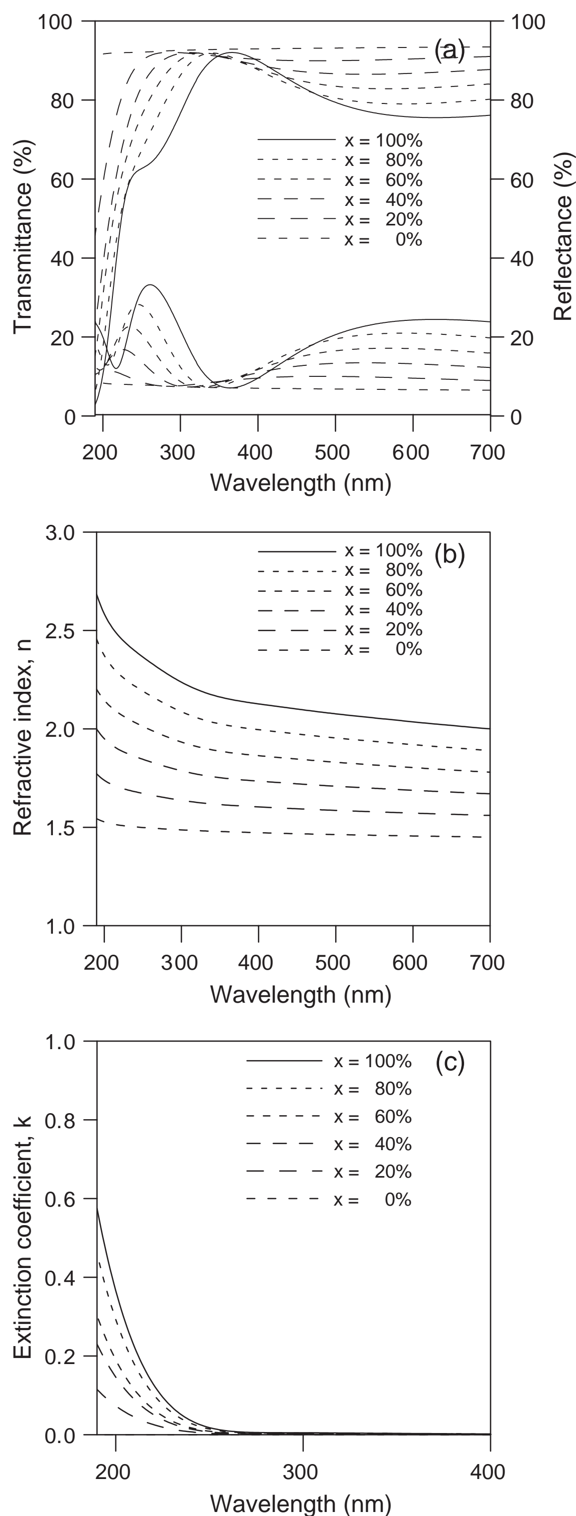


Fig. 1. (a) Measured transmittance and reflectance vs. wavelength. The wavelength dependence of (b) refractive index and (c) extinction coefficient for $(ZrO_2)_x$–$(SiO_2)_{1-x}$ composite films on mole fractions of $ZrO_2$.

Regarding the refractive index of mixed component films, the effective medium approximation for the relationship

between the optical constants and the film composition can usually be modeled using the Lorentz–Lorenz model, the Drude model and the linear model [20]. The EMA results calculated with these models, for various $ZrO_2$ mole fractions, are also shown in Fig. 2. As can be seen, the best agreement with experimental measurements is obtained using the EMA with the linear model. This linear relationship had also been reported by Feldman et al. [20]. A $(ZrO_2)_x$–$(SiO_2)_{1-x}$ composite film that is to be used as a HT-AttPSM blank must have its transmittance of 20±5% in the ArF-exposure-line; we have identified the unique range of $ZrO_2$ mole fraction to be between 30.7% and 62.1% for HT-AttPSM applications.

Our previous report [13] has shown that the optical constants of the $(ZrO_2)_x$–$(Al_2O_3)_{1-x}$ films are linearly dependent on the $ZrO_2$ mole fraction. In ArF lithography, the $ZrO_2$ volume fraction range, necessary to attain the $n$–$k$ values required for an HT-APSM blank with a transmittance of 20±5%, is calculated to be between 37.8% and 66.9% [13].

### *3.3. Optical constants of $(Al_2O_3)_x$–$(ZrO_2)_x$–$(SiO_2)_{1-2x}$ and $(Al_2O_3)_{1-2x}$–$(ZrO_2)_x$–$(SiO_2)_x$ composite films*

Fig. 3(a) shows the refractive indices and extinction coefficients of $(Al_2O_3)_x$–$(ZrO_2)_x$–$(SiO_2)_{1-2x}$ composite films vs. the mole fraction of $SiO_2$ at a wavelength of 193 nm. The refractive indices and extinction coefficients decrease when the $SiO_2$ mole fraction increases. For comparison the results calculated using the three EMA models are also shown in Fig. 3(a). The linear model shows the best agreement between the measured and the calculated refractive indices. The relationship between the extinction coefficient and the $SiO_2$ mole fraction also approaches linear dependence. Fig. 3(b) shows the refractive indices and extinction coefficients of the $(Al_2O_3)_{1-2x}$–$(ZrO_2)_x$–$(SiO_2)_x$ composite films vs. the mole fraction of $Al_2O_3$ at a wavelength of 193 nm. Again, the linear model shows the best agreement between the measured optical constants and the calculated values. Therefore, it is plausible that the optical constants of $(Al_2O_3)_x$–$(ZrO_2)_y$–$(SiO_2)_{1-x-y}$ composite films vary almost linearly as a function of $(x, y)$, the mole fractions of $(Al_2O_3, ZrO_2)$.

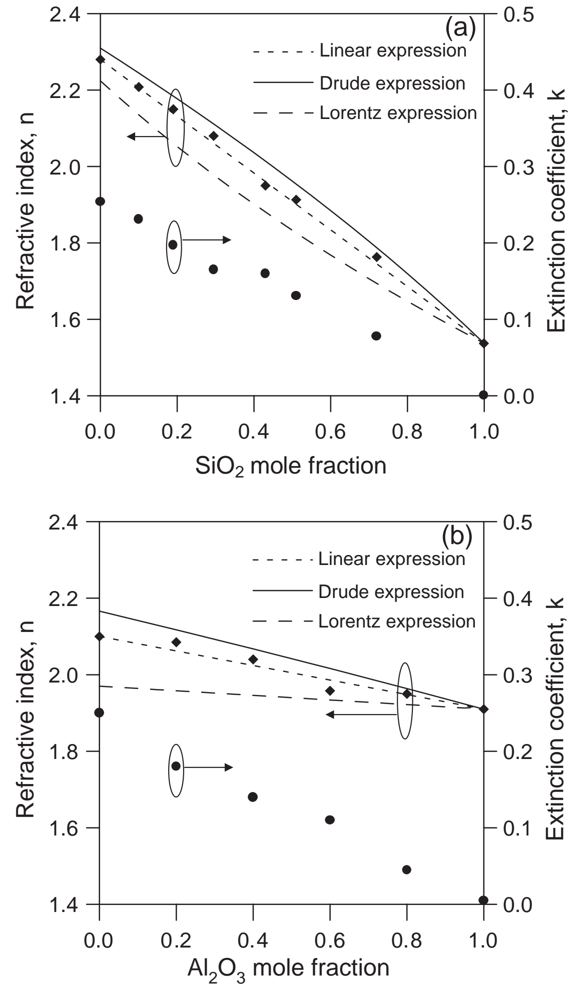


Fig. 3. Refractive indices and extinction coefficients of (a) $(Al_2O_3)_x$–$(ZrO_2)_x$–$(SiO_2)_{1-2x}$ and (b) $(Al_2O_3)_{1-2x}$–$(ZrO_2)_x$–$(SiO_2)_x$ composite films vs. $SiO_2$ mole fraction at 193 nm wavelength. Refractive index varies almost linearly with $SiO_2$ mole fraction. The effective medium approximation results calculated with the Lorentz–Lorenz model, the Drude model and the linear model, for various $ZrO_2$ mole fractions, are also shown.

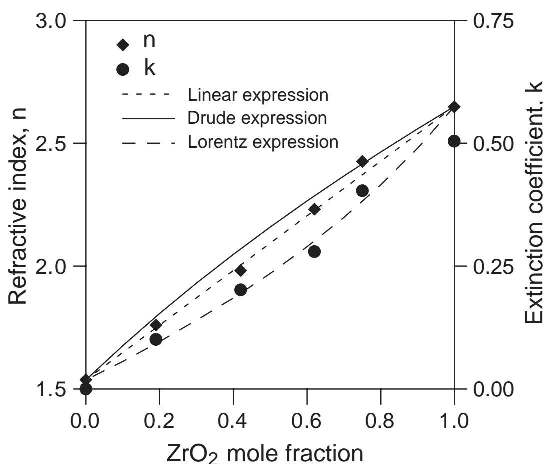


Fig. 2. Refractive index and extinction coefficient vs. $ZrO_2$ mole fraction at 193 nm wavelength for $(ZrO_2)_x$–$(SiO_2)_{1-x}$ composite films represented in Fig. 1(b). The effective medium approximation results calculated with the Lorentz–Lorenz model, the Drude model and the linear model, for various $ZrO_2$ mole fractions, are also shown.

### *3.4. Calculated domain for optical requirements of a HT-AttPSM blank for using in the $(Al_2O_3)_x$–$(ZrO_2)_y$–$(SiO_2)_{1-x-y}$ composite films*

The $(Al_2O_3, ZrO_2)$ mole-fraction-dependent optical constants of $(Al_2O_3)_x$–$(ZrO_2)_y$–$(SiO_2)_{1-x-y}$ composite films are attained as follows:

$$n_{(Al_2O_3)_x+(ZrO_2)_y+(SiO_2)_{1-x-y}} = x \cdot n_{Al_2O_3} + y \cdot n_{ZrO_2} + (1-x-y) \cdot n_{SiO_2},$$

$$k_{(Al_2O_3)_x+(ZrO_2)_y+(SiO_2)_{1-x-y}} = x \cdot k_{Al_2O_3} + y \cdot k_{ZrO_2} + (1-x-y) \cdot k_{SiO_2},$$

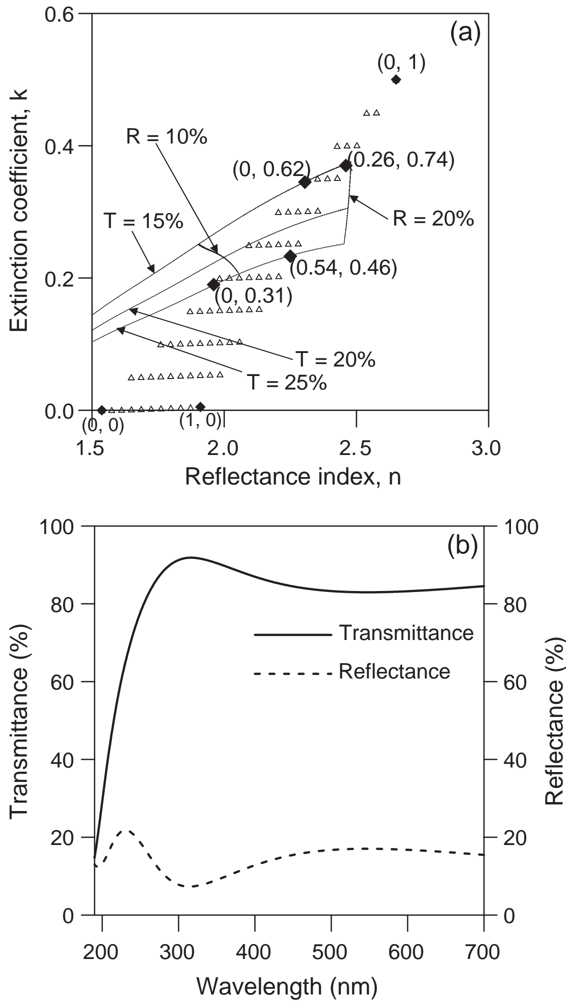


Fig. 4. (a) Calculated optical constants of $(Al_2O_3)_x-(ZrO_2)_y-(SiO_2)_{1-x-y}$ composite films on ($x$, $y$) mole fractions of ($Al_2O_3$, $ZrO_2$) from the measured optical constants of $Al_2O_3$, $ZrO_2$ and $SiO_2$ films as π phase shifters. Calculated domain of mole fraction of ($Al_2O_3$, $ZrO_2$) for $(Al_2O_3)_x-(ZrO_2)_y-(SiO_2)_{1-x-y}$ composite films with transmittance of 20±5% is also shown. The optical requirements for a HT-AttPSM blank are also shown. Indicated in each parenthesis are the refractive index and extinction coefficient. (b) Measured transmittance and reflectance spectra of $(Al_2O_3)_{0.1}-(ZrO_2)_{0.52}-(SiO_2)_{0.38}$ film with the thickness of 82.8 nm.

where $n_{(Al_2O_3)_x+(ZrO_2)_y+(SiO_2)_{1-x-y}}$, $n_{Al_2O_3}$, $n_{ZrO_2}$ and $n_{SiO_2}$, and $k_{(Al_2O_3)x+(ZrO_2)y+(SiO_2)1-x-y}$, $k_{Al_2O_3}$, $k_{ZrO_2}$, and $k_{SiO_2}$ are the refractive indices and the extinction coefficients of $(Al_2O_3)_x-(ZrO_2)_y-(SiO_2)_{1-x-y}$ composite film, $Al_2O_3$ film, $ZrO_2$ film, and $SiO_2$ film, respectively; while $x$ and $y$ are the mole fractions of $Al_2O_3$ and $ZrO_2$, respectively, in the composite films.

The phase shift, which is the phase difference between the deposited film region and the non-deposited film region, can be described as follows:

$$\phi = \frac{2\pi(n-1)d}{\lambda},$$

where $\phi$ is the phase shift; $\lambda$ is the wavelength of 193 nm; $n$ is the refractive index of the film; and $d$ is the thickness of the film.

Let ($x$, $y$) represent an arbitrary point in the $X-Y$ diagram, where $x$ and $y$ refer to the respective mole fractions of $Al_2O_3$ and $ZrO_2$ films in the $(Al_2O_3)_x-(ZrO_2)_y-(SiO_2)_{1-x-y}$ composite films; (0, 0), (1, 0), and (0, 1) indicate, respectively, the points where the 100% mole fraction of $SiO_2$, $Al_2O_3$, and $ZrO_2$, are shown in the $X-Y$ diagram in Fig. 4(a). We can identify a quadrangular area that represents the optical requirements of the $n-k$ value necessary for a HT-AttPSM blank with a transmittance of 20±5%, a reflectance of less than 20% and a phase shift of 180°. This calculated quadrangular area is bounded by (0, 0.31), (0, 0.62), (0.26, 0.74) and (0.54, 0.46) [also shown in Fig. 4(a)]. Therefore, $(Al_2O_3)_x-(ZrO_2)_y-(SiO_2)_{1-x-y}$ composite films, with wide-range tunable optical constants, would be a good candidate for HT-AttPSM applications. When the optical transmittance of a HT-AttPSM is 18–20% [4], ArF lithography has the optimized aerial image. Therefore, a HT-AttPSM blank with the optical transmittance of 19% is anticipated. One $(Al_2O_3)_{0.1}-(ZrO_2)_{0.52}-(SiO_2)_{0.38}$ composite film was successfully fabricated. It had a thickness of 82.8 nm, a transmittance of 18.8%, a reflectance of 12.4%, and a calculated phase shift of 181.8° at 193 nm, as shown in Fig. 4(b). Its optical properties meet the optical requirements of a HT-AttPSM blank [21].

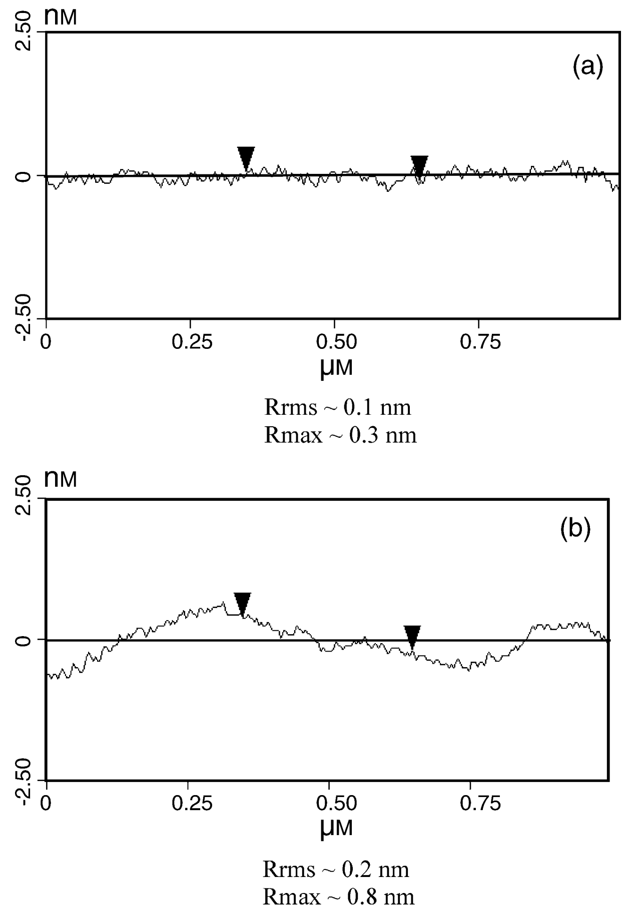


Fig. 5. Surface roughness of $(Al_2O_3)_{0.1}-(ZrO_2)_{0.52}-(SiO_2)_{0.38}$ composite film (a) before and (b) after the chemical durability test. Rrms and Rmax are the root mean square value and the maximum peak to valley magnitude of surface roughness, respectively.

### *3.5. Surface roughness of composite films before and after chemical durability testing*

The root mean square value of the surface roughness before the testing is less than 0.2 nm and the maximum peak to valley magnitude was less than 0.6 nm as shown in Fig. 5(a). Because $(Al_2O_3)_x-(ZrO_2)_y-(SiO_2)_{1-x-y}$ composite films exhibit good chemical inertness, the mean value after the test was less than 0.3 nm and the maximum value was less than 0.9 nm as shown in Fig. 5(b). The film morphology was determined by the scanning electron microscope (SEM) to be very flat and not porous structure. Accordingly, the variation in calculated phase shift was less than 3°, which is within the acceptable range for HT-AttPSM applications [21].

### *3.6. Adhesion test of composite films using adhesive tape testing*

It is very important that HT-AttPSM films adhere well to the fused silica substrate. An investigation, using adhesive tape and the ASTM Crosshatch tape testing method, was carried out on films that were previously deposited on fused silica substrates. All the films passed the adhesion test. This observation suggests the developed optical thin film is a promising and reliable candidate for the HT-AttPSM.

## 4. Conclusion

Mono-layer amorphous $Al_2O_3-ZrO_2-SiO_2$ composite film is a new candidate material for HT-AttPSMs to be utilized in ArF lithography. The optical constants of the $ZrO_2-SiO_2$ composite films are shown to fit the linear EMA model. The optical constants are linearly dependent on the $(x, y)$ mole fractions of $(Al_2O_3, ZrO_2)$ in the $(Al_2O_3)_x-(ZrO_2)_y-(SiO_2)_{1-x-y}$ composite films. It was found that the wide-range tunable optical constants of these $Al_2O_3-ZrO_2-SiO_2$ composite films meet the optical requirements for an HT-AttPSM blank material. One domain of the $(Al_2O_3, ZrO_2)$ mole fraction satisfies the $n-k$ value requirements for a HT-AttPSM blank, which allowed for a transmittance of $20\pm5\%$, a reflectance of less than 15% and a π-phase shift when used in ArF lithography. The calculated bounds are (0, 0.31), (0, 0.62), (0.26, 0.74) and (0.54, 0.46). By controlling the $(x, y)$ mole fractions of $(Al_2O_3, ZrO_2)$, tunable optical constant $(Al_2O_3)_x-(ZrO_2)_y-(SiO_2)_{1-x-y}$ composite films, which satisfy the optical requirements of an HT-AttPSM with an optimized transmittance of 19%, can be easily fabricated. One $(Al_2O_3)_{0.1}-(ZrO_2)_{0.52}-(SiO_2)_{0.38}$ composite film, which was fabricated with a thickness of 82.8 nm, a transmittance of 18.8%, a reflectance of 12.4% and a calculated phase shift of 181.8° at 193 nm, could be used as an ArF-line HT-AttPSM blank. Moreover, all the films met the requirements of surface roughness, before and after the chemical durability test, and the adhesion test.

## Acknowledgements

This research is supported partly by the National Nano Device Laboratories at Taiwan under contract NDT-93S-C096 and partly by the Metals Industry Research and Development Centre at Taiwan under contract 94-0394.

## References

[1] H. Jinbo, Y. Yamashita, Jpn. J. Appl. Phys. 30 (1991) 2998.
[2] H. Watanabe, E. Sugiura, Y. Todokoro, M. Inoue, Jpn. J. Appl. Phys. 30 (1991) 3004.
[3] T. Terasawa, N. Hasegawa, H. Fukuda, S. Katagiri, Jpn. J. Appl. Phys. 30 (1991) 2991.
[4] R.J. Socha, J.S. Petersen, F. Chen, T. Laiding, K. Wampler, R. Caldwell, SPIE Proc. 3546 (1998) 617.
[5] J.S. Petersen, M. McCallum, N. Kachwala, R.J. Scoha, SPIE Proc. 3546 (1998) 288.
[6] B.W. Smith, Z. Alam, S. Butt, S. Kurinec, R.L. Lane, G. Arthur, Microelectron. Eng. 35 (1997) 201.
[7] S. Ito, T. Iwamatsu, H. Sato, M. Asano, K. Kawano, F. Miyashita, J. Vac. Sci. Technol., B 14 (6) (1996) 4199.
[8] E. Kim, S.Y. Moon, Y.H. Kim, H.S. Yoon, K. No, Opt. Eng. 39 (11) (2000) 2947.
[9] T. Matsuo, K. Ohkubo, T. Haraguchi, K. Ueyama, SPIE Proc. 3096 (1997) 354.
[10] P.F. Carcia, R.H. French, M.H. Reilly, M.F. Lemon, D.J. Jones, Appl. Phys. Lett. 70 (1997) 2371.
[11] F.D. Lai, L.A. Wang, Thin Solid Films 409 (2002) 220.
[12] X. Wang, H. Masumoto, Y. Someno, T. Hirai, Thin Solid Films 338 (1999) 105.
[13] Fu-Der Lai, J. Vac. Sci. Technol., B 22 (3) (2004) 1174.
[14] J.V. Stebut, S. Febvay, B. Stauder, J. Lepage, J.M. Brion, B. Sander, G. Pierson, Surf. Coat. Technol. 60 (1993) 458.
[15] E. Dõrre, H. Hubner (Eds.), Alumina: Processing Properties and Applications, Springer, Berlin, 1984.
[16] W.D. Sproul, Surf. Coat. Technol. 49 (1991) 284.
[17] F.-D. Lai, Appl. Surf. Sci. 252 (2005) 996.
[18] P.F. Carcia, R.H. French, K. Sharp, J.S. Meth, B.W. Smith, SPIE Proc. 2884 (1996) 255.
[19] C.D. Wagner, W.M. Riggs, L.E. Davis, J.F. Moulder, G.E. Muilenberg, Handbook of X-ray Photoelectron Spectroscopy, Perkin-Elmer, Minnesota, 1978.
[20] A. Feldman, E.N. Farabaugh, W.K. Haller, D.M. Sanders, R.A. Stempniak, J. Vac. Sci. Technol., A 4 (6) (1986) 2969.
[21] P.F. Carcia, R.H. French, K. Sharp, J.S. Meth, B.W. Smith, SPIE Proc. 2884 (1996) 255.